Journal of Systems Engineering and Electronics
Vol. 33, No. 1, February 2022, pp.210 – 221

Sliding mode control of three-phase AC/DC converters using exponential rate reaching law

JEERANANTASIN Narin and NUNGAM Suksun*

Department of Electrical and Computer Engineering, Faculty of Engineering, King Mongkut's University of Technology North Bangkok, Bangkok 10800, Thailand

Abstract: Sliding mode control (SMC) becomes a common tool in designing robust nonlinear control systems, due to its inherent characteristics such as insensitivity to system uncertainties and fast dynamic response. Two modes are involved in the SMC operation, namely reaching mode and sliding mode. In the reaching mode, the system state is forced to reach the sliding surface in a finite time. The major drawback of the SMC approach is the occurrence of chattering in the sliding mode, which is undesirable in most applications. Generally, the trade-off between chattering reduction and fast reaching time must be considered in the conventional SMC design. This paper proposes SMC design with a novel reaching law called the exponential rate reaching law (ERRL) to reduce chattering, and the control structure of the converter is designed based on the multi-input SMC that is applied to a three-phase AC/DC power converter. The simulation and experimental results show the effectiveness of the proposed technique.

Keywords: exponential rate reaching law (ERRL), multi-input sliding mode control (SMC), chattering reduction, three-phase AC-to-DC converter.

DOI: 10.23919/JSEE.2022.000021

1. Introduction

The three-phase AC/DC converter has become popular nowadays because its control structure is simplified and consists of power semiconductor called insulated gate bipolar transistor (IGBT) which is capable to switch at a high frequency. For example, the applications of this converter in various industries are grid connected power converters, electronic power transformers, and variable-speed drives [1−3]. The typical purpose for control design of this converter is to achieve the following system performances: unity power factor unity, constant DC-output voltage with load changing, capable bidirectional power flow, sinusoidal input currents, regenerative capability, and ripple-free output voltage [4,5].

The control technique can be classified into two types: linear and non-linear control. The drawback of the linear control is to operate at the specified design operating point. Therefore, the converters that are non-linear systems should control via the non-linear control technique. The interested and popular non-linear control technique is sliding mode control (SMC) [6−8], due to its inherent characteristics such as insensitivity to system uncertainties, finite-time convergence, and fast dynamic response. A lot of applications of conventional SMC have been studied, such as electrical drive control [9,10] and magnetic levitation control [11]. This classical SMC control generates a chattering phenomenon that is undesirable for most applications since it may excite the neglected high-frequency unmodeled dynamics (e.g., [12]). The improvement of SMC techniques to overcome chattering has been proposed. Among them is the continuation method, which was reviewed in [13,14]. An application of this method was illustrated in [15], where the discontinuous control function was replaced by a saturated function of continuous control. Another example was presented in [16], where the SMC was applied to the control of a permanent-magnet synchronous motor and the chattering was reduced by using a sigmoid function instead of using the signum function in the control law. Some new techniques for the chattering reduction include the higher-order sliding mode method [17], the complementary sliding mode method [18], and the reaching law (RL) method [19,20]. The RL method is of particular interest. It is based on the fact that the chattering is caused by the imperfection of the reaching process. Therefore, this method focuses on specifying an RL that not only ensures the reaching condition but also controls the chattering level. In this way, the system dynamic during the reaching phase and chattering reduction can be designed. The RL method has now become a systematic approach to the design of the SMC systems.

Manuscript received October 26, 2020.
*Corresponding author.

Three RLs were proposed in [21]. The simplest one is the constant rate RL which contains a constant gain and a signum function. Increasing the gain results in reducing the reaching time, but increasing the chattering. The constant rate RL is improved by adding a proportional rate term, called the constant plus proportional rate RL. This law increases the reaching speed when the distance between the state and the sliding manifold is large. Some application examples of this law can be found in [22] and [23]. The last one is called the power rate RL. This law can eliminate chattering, but the robustness of the system is reduced.

Several new RLs have been introduced. The exponential RL was proposed in [24] to remove the interdependence between the reaching time and the chattering level. An RL using the inverse hyperbolic function was proposed in [25]. An RL with a varying gain was presented in [26] for the permanent magnet synchronous motor (PMSM) speed control. In [27], an enhanced exponential RL was applied to control the permanent magnet synchronous generator (PMSG) wind turbine to improve total harmonic distortion. Although each of the aforementioned RLs has its own merit, it involves complicated mathematical expression. Some of them must be simplified by approximation when implemented.

This paper proposes a new technique to control a three-phase AC/DC converter via SMC. There are two parts to consider, namely control structure and control method. In the literature, including [28], the application of the SMC technique adopts a cascaded control structure for the converter control design. This technique consists of two control loops; the inner loop is current control and the outer loop is voltage control. To achieve the control criteria via the cascaded control structure, the inner loop dynamics must be much faster than the outer loop, demanding a large output capacitance that is not suitable for real commercial applications. Therefore, this paper proposes the multi-input control structure to avoid the constraint of the cascaded control structure. In the part of the control method, a new RL called "exponential rate reaching law" (ERRL) is proposed to reduce the chattering with improving total harmonic distortion (THD), enhancing the robustness in the sliding phase and improving the dynamic of the system in the reaching phase. Based on this RL, a detailed analysis of reaching time and robustness will be described. The application of the proposed RL for a three-phase AC/DC converter will be presented. Finally, simulated and experimental results will be shown.

2. Three-phase AC/DC converter model

The schematic diagram of the three-phase AC/DC power converter is presented in Fig. 1, where R is the phase resistor, L is the phase reactor, C_p is the bus capacitor, R_L is the load resistor, i_{sa}, i_{sb} and i_{sc} are the input current, i_{conv} is the convertor current, i_{Cp} is the capacitor current, i_L is the load current and U_{dc} is the DC voltage. S_k ($k = a, b,$ or c) is the switching function of power switches and $\overline{S}_k$ is the opposite status of S_k.

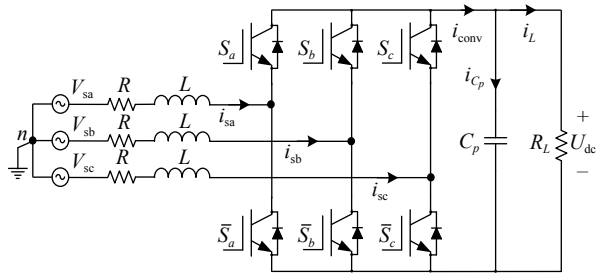

Fig. 1 Three-phase AC/DC converter diagram

The converter is connected to a balanced three-phase source where the phase voltages V_{sa}, V_{sb}, and V_{sc}, are assumed to be (1).

$$\begin{cases} V_{sa} = E_m \cos(\omega t) \\ V_{sb} = E_m \cos\left(\omega t + \dfrac{2\pi}{3}\right) \\ V_{sc} = E_m \cos\left(\omega t - \dfrac{2\pi}{3}\right) \end{cases} \tag{1}$$

It is also assumed that the power switches are loss-free. Hence, the mathematical model of the converter in the synchronously rotating or (d,q) reference frame can be presented as follows:

$$\begin{cases} L\dfrac{\mathrm{d}i_d}{\mathrm{d}t} = v_d - Ri_d + \omega L i_q - f_d U_{dc} \\ L\dfrac{\mathrm{d}i_q}{\mathrm{d}t} = v_q - Ri_q - \omega L i_d - f_q U_{dc} \\ C_p\dfrac{\mathrm{d}U_{dc}}{\mathrm{d}t} = \dfrac{3}{2}(f_d i_d + f_q i_q) - \dfrac{U_{dc}}{R_L} \end{cases} \tag{2}$$

where ω is the supply frequency; i_d, i_q refer to the currents; v_d, v_q refer to the supply voltages, in the (d,q) coordinate frame; f_d, f_q refer to the switching function in the same frame; finally, U_{dc} is the DC voltage. Note that the system (2), with the switching functions f_d and f_q as control variables, are nonlinear. The control design of the power converter is usually aimed at achieving the following system performances, namely unity power factor, sinusoidal input currents, regenerative capability, and ripple-free output voltage.

3. Preliminaries

In this section, we briefly present the theory of SMC design based on the RL method. The theory is based on a

class of nonlinear plants that can be expressed as

$$\dot{\boldsymbol{x}} = \boldsymbol{f}(\boldsymbol{x}) + \boldsymbol{B}(\boldsymbol{x})\boldsymbol{u} \tag{3}$$

where $\boldsymbol{x} = [x_1, x_2, \cdots, x_n]^{\mathrm{T}} \in \mathbf{R}^n$ is the system states vector, $\boldsymbol{f}(\boldsymbol{x}) \in \mathbf{R}^n$ and $\boldsymbol{B}(\boldsymbol{x}) \in \mathbf{R}^{n\times m}$ are nonlinear functions, and $\boldsymbol{u} \in \mathbf{R}^m$ is the control input. Generally, the dynamics of an SMC system consists of two modes, namely reaching mode and sliding mode. The RL-based SMC design begins with the design of sliding mode dynamics, which is done by choosing an appropriate switching function described as

$$\boldsymbol{s} = \boldsymbol{C}^{\mathrm{T}} x = [s_1, s_2, \cdots, s_m]^{\mathrm{T}} \tag{4}$$

where $\boldsymbol{C} \in \mathbf{R}^{n\times m}$ determines the dynamics of the system on the sliding surface $\boldsymbol{s} = \boldsymbol{0}$. The next step is to design the reaching mode dynamics by utilizing an RL. The RL is defined as a differential equation that establishes a reaching condition and directly describes the switching function dynamics. During the reaching mode, the RL forces the system to move from an initial state to the sliding surface in finite time; this time interval is called reaching time. The general form of the RL can be found in [21]. In this section, a special case of the general form called the constant rate RL is chosen to illustrate the design. This law is described as

$$\dot{\boldsymbol{s}} = -\boldsymbol{K}\,\mathbf{sign}(\boldsymbol{s}) \tag{5}$$

where $\boldsymbol{K} = \mathrm{diag}[k_1, k_2, \cdots, k_m]$, $k_i > 0$, $\mathbf{sign} = [\mathrm{sign}(s_1), \mathrm{sign}(s_2), \cdots, \mathrm{sign}(s_m)]^{\mathrm{T}}$, $\mathbf{sign}(\cdot)$ is the signum function.

This RL is conventionally used because of its simplicity. From (4), the time derivative of S along the reaching mode trajectory can be determined as

$$\dot{\boldsymbol{s}} = \frac{\partial \boldsymbol{s}}{\partial \boldsymbol{x}}\dot{\boldsymbol{x}} = \frac{\partial \boldsymbol{s}}{\partial \boldsymbol{x}}[\boldsymbol{f}(\boldsymbol{x}) + \boldsymbol{B}(\boldsymbol{x})\boldsymbol{u}]. \tag{6}$$

The control law can be obtained from (5) and (6) as

$$\boldsymbol{u} = -\left[\frac{\partial \boldsymbol{s}}{\partial \boldsymbol{x}}\boldsymbol{B}(\boldsymbol{x})\right]^{-1}\left[\frac{\partial \boldsymbol{s}}{\partial \boldsymbol{x}}\boldsymbol{f}(\boldsymbol{x}) + \boldsymbol{K}\,\mathbf{sign}(\boldsymbol{s})\right], \tag{7}$$

provided that $\dfrac{\partial \boldsymbol{s}}{\partial \boldsymbol{x}}\boldsymbol{B}(\boldsymbol{x})$ is nonsingular.

The control law in (7) consists of two parts. The first part, called equivalent control, is defined as

$$\boldsymbol{u}_{\mathrm{eq}} = -\left[\frac{\partial \boldsymbol{s}}{\partial \boldsymbol{x}}\boldsymbol{B}(\boldsymbol{x})\right]^{-1}\left[\frac{\partial \boldsymbol{s}}{\partial \boldsymbol{x}}\boldsymbol{f}(\boldsymbol{x})\right]. \tag{8}$$

Using the equivalent control (8) in (3) gives the sliding mode equation of the system. The second part, called discontinuous control, maintains the robustness of the system from the parametric uncertainties and disturbances. Integrating (5) with respect to time results in the reaching time as

$$t_{\mathrm{reach}_i} = \frac{|s_i(0)|}{k_i}, \quad i = 1, 2, \cdots, m. \tag{9}$$

From (9), it is clear that increasing K reduces the reaching time, but the chattering increases. This drawback is due to the fixed gain. The next section discusses the proposed RL to reduce chattering.

4. SMC with ERRL

A new RL, called ERRL, is described in this section. The proposed ERRL is described in vector format as

$$\dot{\boldsymbol{s}} = -\boldsymbol{K}\boldsymbol{\rho}(\boldsymbol{s}, \mu, \sigma)\mathbf{sign}(\boldsymbol{s}) \tag{10}$$

where σ is a positive integer, $0 < \sigma < 1$; μ is a positive integer, $0 < \mu < 1$; $\boldsymbol{K} = \mathrm{diag}[k_1, k_2, \cdots, k_m]$, $k_i > 0$; $\boldsymbol{\rho}(\boldsymbol{s},\mu,\sigma) = \mathrm{diag}[(1-\mu \mathrm{e}^{-|s_1|/\sigma_i}), \cdots, (1-\mu \mathrm{e}^{-|s_m|/\sigma_i})]$; $\mathbf{sign} = [\mathrm{sign}(s_1), \mathrm{sign}(s_2), \cdots, \mathrm{sign}(s_m)]^{\mathrm{T}}$.

The scalar format of (10) can also be written as

$$\dot{s}_i = -k_i(1 - \mu_i \mathrm{e}^{-\frac{|s_i|}{\sigma_i}})\mathrm{sign}(s_i), \quad i = 1, 2, \cdots, m. \tag{11}$$

The reaching time t_{reach_i} for s_i can be determined by rearranging (11) as

$$\dot{s}_i(1 - \mu_i \mathrm{e}^{-\frac{|s_i|}{\sigma_i}})^{-1} = -k_i \mathrm{sign}(s_i(t)). \tag{12}$$

By integrating (12) with respect to time, the reaching time is obtained as

$$t_{\mathrm{reach}_i} = -\frac{1}{k_i}\int_0^{s_i(0)} (1 - \mu_i \mathrm{e}^{-\frac{|s_i|}{\sigma_i}})^{-1} \mathrm{sign}(s_i(t))\,\mathrm{d}s. \tag{13}$$

From (13), when $\mathrm{sign}(s_i(t)) < 0$, we obtain

$$t_{\mathrm{reach}_i} = \frac{1}{k_i}\int_0^{s_i(0)} (1 - \mu_i \mathrm{e}^{-\frac{|s_i|}{\sigma_i}})^{-1}\,\mathrm{d}s \tag{14}$$

and when $\mathrm{sign}(s_i(t)) > 0$, we obtain

$$t_{\mathrm{reach}_i} = \frac{1}{k_i}\int_0^{-s_i(0)} (1 - \mu_i \mathrm{e}^{-\frac{|s_i|}{\sigma_i}})^{-1}\,\mathrm{d}s. \tag{15}$$

From (14) and (15), it can be concluded that

$$t_{\mathrm{reach}_i} = \frac{1}{k_i}\int_0^{|s_i(0)|} (1 - \mu_i \mathrm{e}^{-\frac{|s_i|}{\sigma_i}})^{-1}\,\mathrm{d}s. \tag{16}$$

From (16) we finally obtain

$$t_{\mathrm{reach}_i} = \frac{\sigma_i}{k_i}\ln\left|\frac{\mathrm{e}^{|s_i(0)|/\sigma_i} - \mu_i}{1 - \mu_i}\right|. \tag{17}$$

The proposed RL as given in (11) can be considered as an RL with an adaptative gain where the term $1 - \mu \mathrm{e}^{-|s|/\sigma}$ may be thought as an adjustable coefficient of K. For a large value of S, meaning that the state is very far from the sliding surface, this term converges to unity. This gives rise to a very fast reaching speed which is determined by K. As the system trajectory approaches the sliding surface, this term gradually decreases to $1 - \mu$ which is less than unity. Hence the chattering can be influenced by the choice of μ: increasing the value of μ reduces the

chattering level. The effect of σ on chattering can also be concluded by the same analysis: decreasing the value of σ increases the chattering level. Although both μ and σ affect chattering and reaching time, the fact that σ appears explicitly on reaching time equation as presented in (17) makes σ the obvious choice for specifying the reaching time, leaving μ for determining the trade-off between the chattering reduction and robustness.

By following the same procedure as described in Section 2, the control law of the proposed RL can be expressed as

$$\boldsymbol{u} = -\left[\frac{\partial \boldsymbol{s}}{\partial \boldsymbol{x}}\boldsymbol{B}\right]^{-1}\left[\frac{\partial \boldsymbol{s}}{\partial \boldsymbol{x}}\boldsymbol{f}(\boldsymbol{x}) + \boldsymbol{K}\boldsymbol{\rho}(\boldsymbol{s},\mu,\sigma)\mathbf{sign}(\boldsymbol{s})\right]. \quad (18)$$

Notice that (7) and (18) give the same equivalent control, indicating that the dynamics on the sliding mode of both systems are identical. However, the proposed RL can reduce chattering by a choice of its parameters.

5. Reaching condition under system perturbations

This section presents an analysis of the ERRL under the system perturbations. Let us assume that the terms $\boldsymbol{f}(\boldsymbol{x})$ and $\boldsymbol{B}(\boldsymbol{x})$ of the nonlinear system expressed in (3) are not exactly known, but approximated as $\hat{\boldsymbol{f}}(\boldsymbol{x})$ and $\hat{\boldsymbol{B}}(\boldsymbol{x})$, respectively. Furthermore, we assume that the matrix $\boldsymbol{C}$ is constant. From (6), the sliding surface is obtained as

$$\dot{\boldsymbol{s}}(t) = \boldsymbol{C}^{\mathrm{T}}\boldsymbol{f}(\boldsymbol{x}) + \boldsymbol{C}^{\mathrm{T}}\boldsymbol{B}(\boldsymbol{x})\boldsymbol{u}. \quad (19)$$

Therefore, the control input is able to be determined from the RL as presented in (10) under the condition $\dot{\boldsymbol{s}}(t) = \boldsymbol{0}$ as

$$\hat{\boldsymbol{u}} = -(\boldsymbol{C}^{\mathrm{T}}\boldsymbol{B}(\boldsymbol{x}))^{-1}\left[\boldsymbol{C}^{\mathrm{T}}\boldsymbol{f}(\boldsymbol{x}) + \boldsymbol{K}\boldsymbol{\rho}(\boldsymbol{s},\mu,\sigma)\mathbf{sign}(\boldsymbol{s})\right] \quad (20)$$

where $\hat{\boldsymbol{u}}$ is the control input for the nominal $\hat{\boldsymbol{f}}(\boldsymbol{x})$ plant and $\hat{\boldsymbol{B}}(\boldsymbol{x})$. By substituting (20) into (19), we obtain

$$\dot{\boldsymbol{s}} = \boldsymbol{C}^{\mathrm{T}}\boldsymbol{f}(\boldsymbol{x}) - \boldsymbol{C}^{\mathrm{T}}\boldsymbol{B}(\boldsymbol{x})((\boldsymbol{C}^{\mathrm{T}}\hat{\boldsymbol{B}}(\boldsymbol{x}))^{-1}(\boldsymbol{C}^{\mathrm{T}}\hat{\boldsymbol{f}}(\boldsymbol{x}) + \boldsymbol{K}\boldsymbol{\rho}(\boldsymbol{s},\mu,\sigma)\mathbf{sign}(\boldsymbol{s}))). \quad (21)$$

Let

$$\boldsymbol{V}(\boldsymbol{s}) = \frac{1}{2}\boldsymbol{s}^{\mathrm{T}}\boldsymbol{s} \quad (22)$$

be a Lyapunov function candidate. The reaching condition can be found as

$$\dot{\boldsymbol{V}}(\boldsymbol{s}) = \boldsymbol{s}^{\mathrm{T}}\dot{\boldsymbol{s}} < 0. \quad (23)$$

Hence, from (21), we have

$$\boldsymbol{s}^{\mathrm{T}}\dot{\boldsymbol{s}} = \boldsymbol{s}^{\mathrm{T}}(\boldsymbol{C}^{\mathrm{T}}\boldsymbol{f}(\boldsymbol{x}) - \boldsymbol{Z}\boldsymbol{C}^{\mathrm{T}}\hat{\boldsymbol{f}}(\boldsymbol{x}) - \boldsymbol{P}\mathbf{sign}(\boldsymbol{s})) = \boldsymbol{s}^{\mathrm{T}}\left(\boldsymbol{C}^{\mathrm{T}}\boldsymbol{f}(\boldsymbol{x}) - \boldsymbol{Z}\boldsymbol{C}^{\mathrm{T}}\hat{\boldsymbol{f}}(\boldsymbol{x}) - \boldsymbol{P}\frac{\boldsymbol{s}}{\|\boldsymbol{s}\|}\right) \quad (24)$$

where $\boldsymbol{Z} = \boldsymbol{C}^{\mathrm{T}}\boldsymbol{B}(\boldsymbol{x})(\boldsymbol{C}^{\mathrm{T}}\hat{\boldsymbol{B}}(\boldsymbol{x}))^{-1}$, $\boldsymbol{P} = \boldsymbol{Z}\boldsymbol{K}\boldsymbol{\rho}(\boldsymbol{s},\mu,\sigma)$ and $\boldsymbol{s}/|\boldsymbol{s}| = [\boldsymbol{s}_1/|\boldsymbol{s}_1|\ \boldsymbol{s}_2/|\boldsymbol{s}_2|,\cdots,\boldsymbol{s}_m/|\boldsymbol{s}_m|]^{\mathrm{T}}$. Assuming that $\boldsymbol{Z}$ and $\boldsymbol{P}$ are diagonal, then the reaching condition (23) is fulfilled if

$$p_{i,i} > \left|\boldsymbol{C}^{\mathrm{T}}\boldsymbol{f}(\boldsymbol{x}) - \boldsymbol{Z}\boldsymbol{C}^{\mathrm{T}}\hat{\boldsymbol{f}}(\boldsymbol{x})\right|_i \quad (25)$$

where $p_{i,i}$ is the element (i,i) of P, and $i = 1, 2,\cdots,m$. The condition (25) will be used in Section 6 for the choice of K that satisfies the reaching condition under system perturbations.

6. ERRL-based control design for the converter

The proposed SMC design via a multi-input control structure in Fig. 2 is developed with reference to the steady-state conditions described in this subsection. In Fig. 2, SVPWM refers to the space vector pulse width modulation. K_{udc} is a gain constant to compensate input voltage.

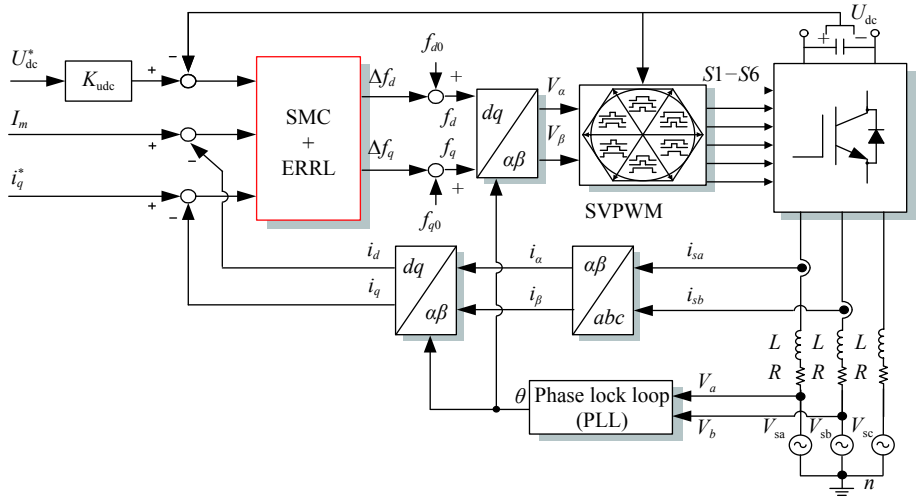

Fig. 2 Control structure of the three-phase converter

In an ideal steady-state, the DC output voltage is maintained at a reference voltage, $U_{\rm dc}^*$. Since i_q is controlled to zero to obtain unity power factor, i_d equals the magnitude of the input line I_m. Let f_{d0} and f_{q0} be defined as the switching function f_d and f_q at steady-state, respectively. From (2), with $U_{\rm dc}=U_{\rm dc}^*$, $i_d^*=I_m$, $i_q=0$, $f_d=f_{d0}$, $f_q=f_{q0}$ and all derivative terms set to zero, the system at steady-state can be described as expressed in (26), (27) and (28).

$$RI_m + f_{d0}U_{\rm dc}^* = E_m \tag{26}$$

$$\omega L I_m + f_{q0}U_{\rm dc}^* = 0 \tag{27}$$

$$\frac{3}{2}f_{d0}I_m = I_L \tag{28}$$

From (26) and (27), the switching function at steady-state can be obtained as

$$f_{d0} = \frac{E_m - RI_m}{U_{\rm dc}^*}, \tag{29}$$

$$f_{q0} = \frac{-\omega L I_m}{U_{\rm dc}^*}. \tag{30}$$

By substituting (29) into (28), the load current can be expressed as

$$I_L = \frac{3}{2U_{\rm dc}^*}(E_m I_m - RI_m^2). \tag{31}$$

The current I_m can be determined from (31) as

$$I_m = \frac{1}{2}\left[\frac{E_m}{R} \pm \sqrt{\left(\frac{E_m}{R}\right)^2 - \frac{8U_{\rm dc}^* I_L}{3R}}\right]. \tag{32}$$

From (32), there are two values of I_m for a given load current. While the smaller value of I_m is always used in the control design, whether or not the larger one can also be used depends on the operating point of the converter; more detail can be found in [29]. In the development of the design described in the next section, we assume that the converter is connected to a resistive load, R_L; hence I_L in (32) is determined by $U_{\rm dc}^*/R_L$.

According to the multi-input control structure, the errors between the references and the actual variable values are new state variables as defined in (33), where $i_d^* = I_m$, $i_q^* = 0$, and $U_{\rm dc}^*$ are the references with respect to the steady-state conditions discussed above.

$$\begin{cases} e_d = i_d^* - i_d \\ e_q = i_q^* - i_q \\ e_{\rm udc} = U_{\rm dc}^* - U_{\rm dc} \end{cases} \tag{33}$$

These state variables can be written in the form of (3), where

$$\boldsymbol{x} = \begin{bmatrix} x_d \\ x_q \\ x_{\rm udc} \end{bmatrix} = \begin{bmatrix} e_d \\ e_q \\ e_{\rm udc} \end{bmatrix} = \boldsymbol{e},$$

$$\dot{\boldsymbol{x}} = \dot{\boldsymbol{e}} = \begin{bmatrix} \dot{e}_d \\ \dot{e}_q \\ \dot{e}_{\rm udc} \end{bmatrix},$$

$$\boldsymbol{f}(\boldsymbol{x}) = \boldsymbol{f}(\boldsymbol{e}) = \begin{bmatrix} \dot{I}_m - \dfrac{v_d}{L} + \dfrac{R}{L}(e_d) + \dfrac{R}{L}I_m - \omega(e_q) - \omega i_q^* + \dfrac{-e_{\rm udc} + U_{\rm dc}^*}{L}f_{d0} \\ \dot{I}_q^* - \dfrac{v_q}{L} - \dfrac{R}{L}(e_q) + \dfrac{R}{L}i_q^* - \omega(e_d) + \omega I_m + \dfrac{-e_{\rm udc} + U_{\rm dc}^*}{L}f_{q0} \\ \dot{U}_{\rm dc}^* - \dfrac{3}{2C_p}\left(\dfrac{v_d(-e_d + I_m) + v_q\left(-e_q + i_q^*\right)}{-e_{\rm udc} + U_{\rm dc}^*}\right) + \dfrac{(-e_{\rm udc} + U_{\rm dc}^*)}{R_L C_p} \end{bmatrix},$$

$$\boldsymbol{B}(\boldsymbol{x}) = \boldsymbol{B}(\boldsymbol{e}) = \begin{bmatrix} \dfrac{-e_{\rm udc} + U_{\rm dc}^*}{L} & 0 \\ 0 & \dfrac{-e_{\rm udc} + U_{\rm dc}^*}{L} \\ 0 & 0 \end{bmatrix},$$

$$\boldsymbol{u} = \begin{bmatrix} u_d \\ u_q \end{bmatrix} = \begin{bmatrix} \Delta f_d \\ \Delta f_q \end{bmatrix}. \tag{34}$$

The sliding surface based on (4) is chosen as follows:

$$\boldsymbol{s} = \begin{bmatrix} s_d \\ s_q \end{bmatrix} = \begin{bmatrix} c_{11} & 0 & c_{13} \\ 0 & c_{22} & 0 \end{bmatrix}\begin{bmatrix} e_d \\ e_q \\ e_{\rm udc} \end{bmatrix} \tag{35}$$

where c_{11}, c_{13} and c_{22} are constants. In the sliding mode, the condition $s_q = c_{22}e_q = 0$ ensures that i_q is zero, and the condition $s_d = c_{11}e_d + c_{13}e_{\rm udc} = 0$ determines the dynamics of $U_{\rm dc}$; in fact $U_{\rm dc}$ can be described by a stable first-order nonlinear equation, as will appear in the sequel. Substituting (34) and (35) into the control law of the proposed

ERRL as presented in (18), so the control input can be determined as shown in (36).

$$\Delta f_d = \frac{L}{e_{\mathrm{udc}} - U^*_{\mathrm{dc}}}\left[\dot{I}_m - \frac{v_d}{L} + \frac{R}{L}e_d + \frac{R}{L}I_m - \omega e_q - \omega i^*_q + \frac{c_{13}}{c_{11}}\left(\dot{U}^*_{\mathrm{dc}} + \frac{3(v_d(-e_d + I_m) + (v_q(-e_q + I^*_q))}{2C_p(-e_{\mathrm{udc}} + U^*_{\mathrm{dc}})} + \frac{(-e_{\mathrm{udc}} + U^*_{\mathrm{dc}})}{R_L C_p}\right) + \frac{1}{c_{11}}\left(k_d(1 - \mu \mathrm{e}^{-|s_d|/\sigma})\mathrm{sign}(s_d)\right)\right] - \left(\frac{E_m - RI_m}{U^*_{dc}}\right),$$

$$\Delta f_q = \frac{L}{e_{\mathrm{udc}} - U^*_{\mathrm{dc}}}\left[\dot{i}^*_q - \frac{v_q}{L} - \frac{R}{L}e_q + \frac{R}{L}i^*_q - \omega e_d + \omega I_m + \frac{1}{c_{22}}\left(k_q(1 - \mu \mathrm{e}^{-|s_q|/\sigma})\mathrm{sign}(s_q)\right)\right] - \left(\frac{-\omega L I_m}{U^*_{\mathrm{dc}}}\right). \quad (36)$$

Then (36) is substituted into (34) and (35) sequentially and the result is expressed in (37). Hence, the ratio of c_{11} and c_{13} represents the control performance of the system brought about to determine the time constant and the steady-state error of U_{dc}.

$$\dot{U}_{\mathrm{dc}} = -\frac{c_{11}}{c_{13}}\left(\frac{1}{R_L C_p}U_{\mathrm{dc}} - \frac{3v_d I_m}{2C_p U_{\mathrm{dc}}}\right) \quad (37)$$

From (37), the output voltage at steady-state can be determined by setting $\dot{U}_{dc} = 0$ as presented in (38).

$$U_{\mathrm{dc\_}ss} = \pm\sqrt{\frac{3}{2}I_m R_L v_d}. \quad (38)$$

Let us define

$$f(U_{\mathrm{dc}}) = -A_1 U_{\mathrm{dc}} + A_2\frac{1}{U_{\mathrm{dc}}} \quad (39)$$

where $A_1 = \frac{c_{11}}{c_{13}}\frac{1}{R_L C_p}$ and $A_2 = \frac{c_{11}}{c_{13}}\frac{3v_d I_m}{2C_p}$, because

$$\frac{\partial f(U_{\mathrm{dc}})}{U_{\mathrm{dc}}} = -A_1 - A_2\frac{1}{U^2_{\mathrm{dc}}} < 0 \quad (40)$$

which is always negative, except at $U_{\mathrm{dc}} = 0$. From the contraction theorem, the solution goes to $U_{\mathrm{dc\_}ss}$. Considering the chosen sliding surface as in (35), it shows that the steady-state errors of the system still occur. Therefore, the output voltage tracking to the given voltage reference without errors can be achieved by adjusting the gain of the input reference as presented in (41).

$$K_{\mathrm{udc}} = \frac{U^*_{\mathrm{dc}}}{U_{\mathrm{dc\_}ss}} \quad (41)$$

The obtained control input signifies the proposed RL to achieve a power factor close to unity and to decrease chattering. The gain value can be evaluated based on (25) as shown in (42).

$$\begin{cases} k_d > \left|\left(\frac{1}{R_L} - \frac{1}{\hat{R}_L}\right)\frac{U_{\mathrm{dc}}}{C_p}\right|\left(\frac{1}{1 - \mu \mathrm{e}^{-|s_d|/\sigma}}\right) \\ k_q > 0 \end{cases} \quad (42)$$

Considering the s_i function as presented in (42), the term $1 - \mu \mathrm{e}^{-|s_i|/\sigma}$ is the maximum when s_i is given to be zero, which causes the gain K to increase. On the other hand, the increasing or decreasing s_i is not significant to this term $1 - \mu \mathrm{e}^{-|s_i|/\sigma}$, it still decreases and also causes the gain K to decrease. The gain K evaluated from the proposed RL is the sufficient condition to indicate the system robustness to the external perturbations under the specified bound of the uncertainty.

7. Steady-state error reduction

According to the considered first-order system, as abovementioned, the effectiveness and the robustness of the control system without any steady-state error can only be achieved if there is no variation of the load and the parameters. However in the actual system these variations depend on the normal plant operation that has effect on the steady-state error of the current i_q and the output voltage. Therefore, to solve this problem, this study proposes a technique which consists of two steps as shown below:

Step 1 Adding integral term

In this step, the state error e_{q2} that consists of integral term is added into (34) to guarantee that current i_q is zero at steady-state as shown in (43).

$$\boldsymbol{x} = \begin{bmatrix} x_d \\ x_q \\ x_{udc} \\ x_{q2} \end{bmatrix} = \begin{bmatrix} e_d \\ e_q \\ e_{udc} \\ e_{q2} \end{bmatrix} = \boldsymbol{e},$$

$$\dot{\boldsymbol{x}} = \dot{\boldsymbol{e}} = \begin{bmatrix} \dot{e}_d \\ \dot{e}_q \\ \dot{e}_{udc} \\ \dot{e}_{q2} \end{bmatrix},$$

$$\boldsymbol{f}(\boldsymbol{x}) = \boldsymbol{f}(\boldsymbol{e}) = \begin{bmatrix} \dot{I}_m - \frac{v_d}{L} + \frac{R}{L}(e_d) + \frac{R}{L}I_m - \omega(e_q) - \omega i^*_q + \frac{-e_{\mathrm{udc}} + U^*_{\mathrm{dc}}}{L}f_{d0} \\ \dot{I}^*_q - \frac{v_q}{L} - \frac{R}{L}(e_q) + \frac{R}{L}i^*_q - \omega(e_d) - \omega I_m + \frac{-e_{\mathrm{udc}} + U^*_{\mathrm{dc}}}{L}f_{q0} \\ \dot{U}^*_{\mathrm{dc}} - \frac{3}{2C_p}\left(\frac{v_d(-e_d + I_m) + v_q(-e_q + i^*_q)}{-e_{\mathrm{udc}} + U^*_{\mathrm{dc}}}\right) + \frac{(-e_{\mathrm{udc}} + U^*_{\mathrm{dc}})}{R_L C_p} \\ e_q \end{bmatrix}$$

$$\boldsymbol{B}(\boldsymbol{x}) = \boldsymbol{B}(\boldsymbol{e}) = \begin{bmatrix} \frac{-e_{\mathrm{udc}} + U^*_{\mathrm{dc}}}{L} & 0 \\ 0 & \frac{-e_{\mathrm{udc}} + U^*_{\mathrm{dc}}}{L} \\ 0 & 0 \\ 0 & 0 \end{bmatrix},$$

$$\boldsymbol{u}=\begin{bmatrix} u_d \\ u_q \end{bmatrix}=\begin{bmatrix} \Delta f_d \\ \Delta f_q \end{bmatrix}, \tag{43}$$

where $e_{q2}=\int e_q \mathrm{d}t$ and the sliding surface equation can be defined as

$$\begin{cases} s_d = c_{11}e_d + c_{13}e_{\mathrm{udc}} = 0 \\ s_q = c_{22}e_q + c_{24}e_{q2} = c_{22}\dot{e}_q + c_{24}e_q = 0 \end{cases}. \tag{44}$$

Substituting (43) and (44) into the control law of the proposed ERRL as presented in (18), so the control input can be determined as shown in (45).

$$\begin{cases} \Delta f_d = \dfrac{L}{e_{\mathrm{udc}}-U_{\mathrm{dc}}^*}\left[(\dot{I}_m - \dfrac{v_d}{L}+\dfrac{R}{L}e_d+\dfrac{R}{L}I_m-\omega e_q-\omega i_q^*)+\right. \\ \quad \dfrac{c_{13}}{c_{11}}\left(\dot{U}_{\mathrm{dc}}^*+\dfrac{3(v_d(-e_d+I_m^*)+(v_q(-e_q+I_q^*))}{2C_p(-e_{\mathrm{udc}}+U_{\mathrm{dc}}^*)}+\right. \\ \quad \left.\left.\dfrac{(-e_{\mathrm{udc}}+U_{\mathrm{dc}}^*)}{R_LC_p}\right)+\dfrac{1}{c_{11}}(k_d(1-\mu\mathrm{e}^{-|s_d|/\sigma})\mathrm{sign}(s_d))\right]- \\ \quad \left(\dfrac{E_m-RI_m}{U_{\mathrm{dc}}^*}\right) \\ \Delta f_q = \dfrac{L}{e_{\mathrm{udc}}-U_{\mathrm{dc}}^*}\left[\dot{i}_q^*-\dfrac{v_q}{L}-\dfrac{R}{L}e_q+\dfrac{R}{L}i_q^*-\omega e_d+\omega I_m+\right. \\ \quad \left.\dfrac{c_{24}}{c_{22}}e_q+\dfrac{1}{c_{22}}(k_q(1-\mu\mathrm{e}^{-|s_q|/\sigma})\mathrm{sign}(s_q))\right]-\left(\dfrac{-\omega LI_m}{U_{\mathrm{dc}}^*}\right) \end{cases} \tag{45}$$

Therefore, the integral term added in the sliding surface equation causes the elimination of steady-state error in current i_q.

Step 2 Load current compensation

In the normal plant operation, the steady-state error of the output voltage can occur because of the load changing. However, this error in the output voltage U_{dc} can be eliminated by load current compensation. Therefore, the estimation of the load current $\hat{I}_L$ is proposed in (46). The control structure for load current compensation is shown in Fig. 3.

$$I_m=\frac{1}{2}\left[\frac{E_m}{R}\pm\sqrt{\left(\frac{E_m}{R}\right)^2-\frac{8U_{\mathrm{dc}}^*\hat{I}_L}{3R}}\right] \tag{46}$$

where

$$\Delta I_L=\frac{K_I(U_{\mathrm{dc}}^*-U_{\mathrm{dc}})}{s}. \tag{47}$$

Referring to (47), the value of the compensated load current can be determined as

$$\hat{I}_L=\hat{I}_L^*+\Delta I_L. \tag{48}$$

Therefore, the compensation of the load current in order to eliminate the steady-state error of the output voltage during load change can assist in controling the output voltage to equal the reference voltage.

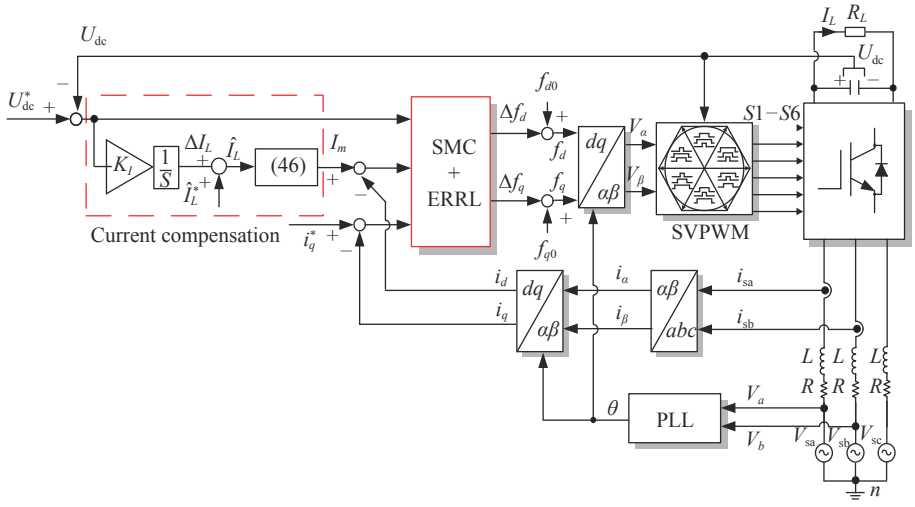

Fig. 3 Block diagram of load current compensation

8. Simulation and experimental results

In order to verify the performance of the proposed SMC method to control three-phase AC/DC converters, the simulations are implemented in Matlab-Simulink and the experimental setup is built as shown in Fig. 4. The parameters which are setup for both simulation and experimentation are listed in Table 1. At the conditions of the AC side, the AC input voltage is default at 90 V with a frequency of 50 Hz. The SVPWM switching frequency is specified at 10 kHz. At the initial operation, the three-phase converter control is connected to load at 300 Ω and the DC output voltage is maintained at step reference U_{dc}^* of 300 V. The i_q is controlled to zero to obtain a unity power factor. Then, after the state reaches the steady-state, the load resistance is changed to 150 Ω. The gain of ERRL is $\sigma=0.7$ and $\mu=0.8$.

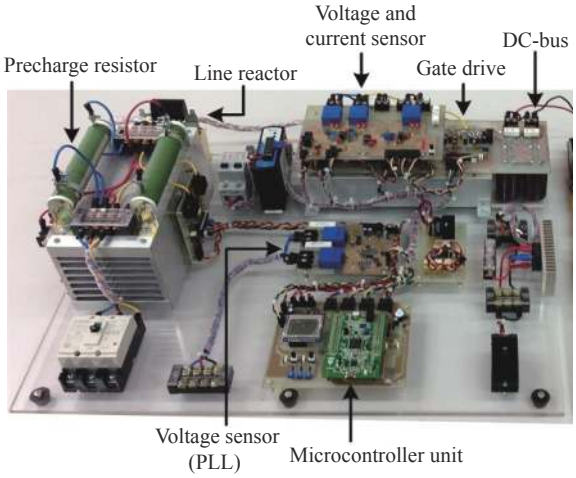

Fig. 4 Experiment setup

Table 1 Parameters of the three-phase converter system

Symbol	Description	Value
$V_{sa,sb,sc}$/V_{rms}	Phase voltage	90
H_z/Hz	Frequency	50
f_s/kHz	Switching frequency	10
R, R_L/Ω	Phase and load resistor	0.8, 300
C/μF	DC bus capacitor	820
L/(mH/Phase)	Phase reactor	4.9

The simulation results of DC output voltage and current line waveform in steady-state period of the converter, when the load of the system is changed from 300 Ω to 150 Ω, are presented in Fig. 5 and Fig. 6, respectively. It is found when the load of the system is changed from 300 Ω to 150 Ω, the output voltage of the system is decreased. Furthermore, the dynamic response in transient period of the changed load is very fast to the steady-state without overshoot as presented in Fig. 7 and Fig. 8. This is the characteristic property of the SMC that its order is reduced to the first order.

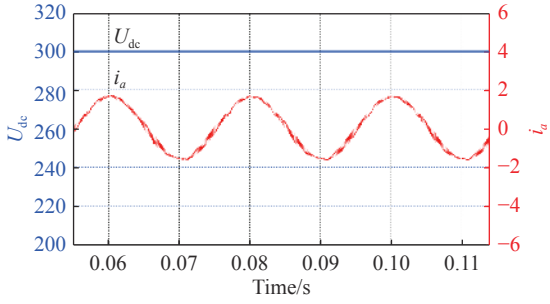

Fig. 5 DC output voltage and line current with load at 300 Ω

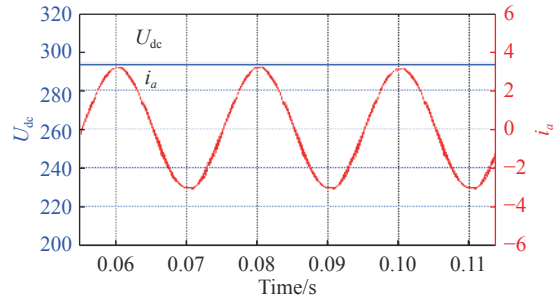

Fig. 6 DC output voltage and line current with load at 150 Ω

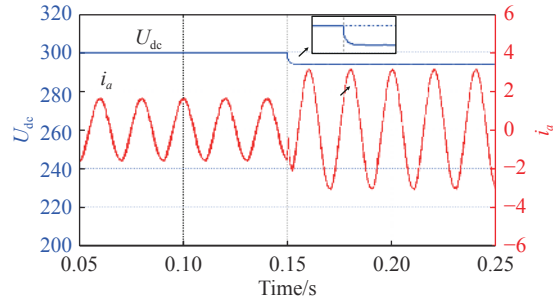

Fig. 7 DC output voltage and line current with load from 300 Ω to 150 Ω

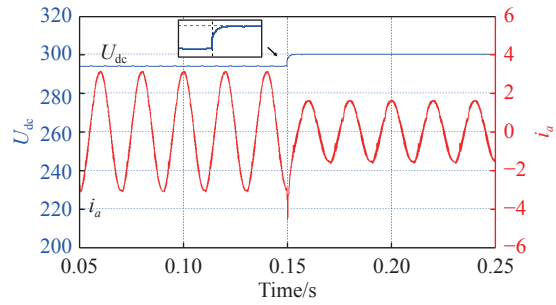

Fig. 8 DC output voltage and line current with load from 150 Ω to 300 Ω

Fig. 9 shows the simulation result of phase voltage and phase input at the constant load 300 Ω. It indicates that the system can be operated at a unity power factor due to the in-phase of the voltage and current waveforms. Fig. 10 and Fig. 11 demonstrate the simulated results of DC output voltage and current line waveform of the converter with the compensated load current method. The compensated load current method can eliminate the steady state error as presented in Fig. 10 and it can be also found that the in-phase of voltage and current waveforms occur at the constant load 300 Ω as presented in Fig. 11.

The simulation results of the current input at a fundamental frequency of 50 Hz to study the effectiveness of the conventional SMC method and the proposed SMC method to reduce the chattering of the system are presented in Fig. 12 and Fig. 13, respectively.

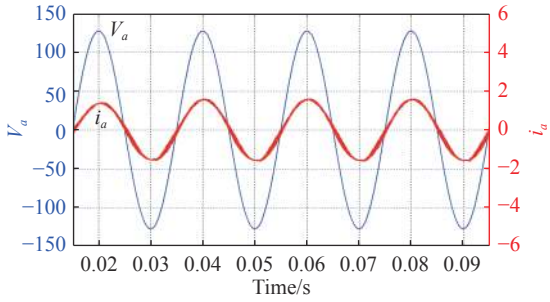

Fig. 9 Phase voltage and phase current input with load at 300 Ω

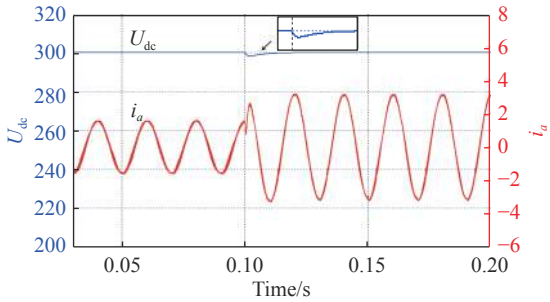

Fig. 10 DC output voltage and line current of the converter with compensated load current method

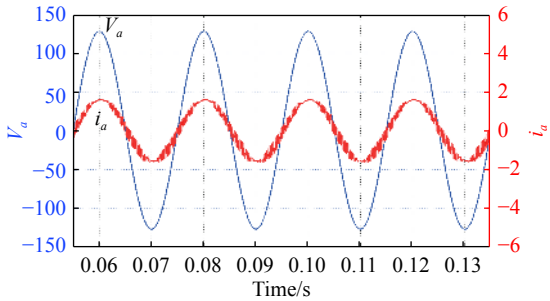

Fig. 11 Phase voltage and phase current input with load at 300 Ω with compensated load current method

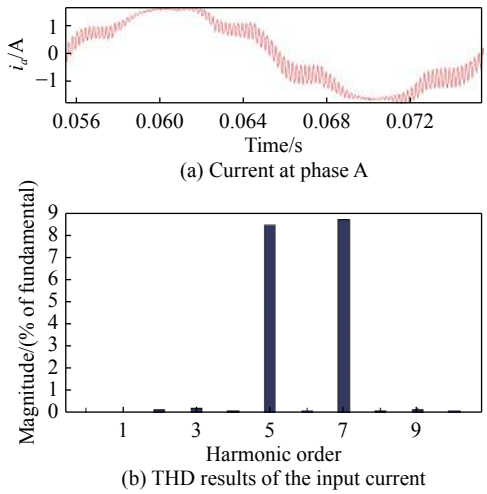

Fig. 12 Conventional control (Fundamental (50Hz)=1.582, THD= 19.62%)

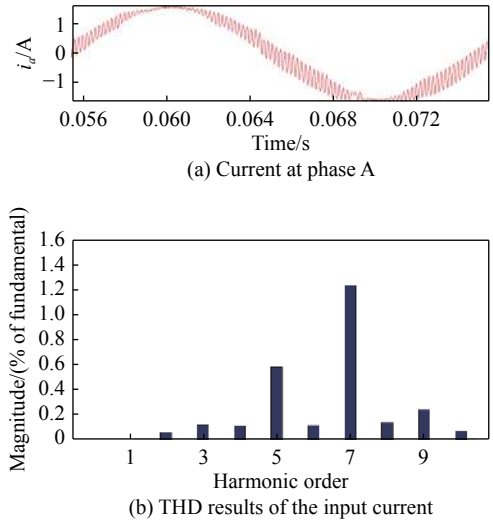

Fig. 13 Proposed method (Fundamental (50 Hz) =1.569, THD = 15.46%)

The effectiveness of the proposed SMC method to decrease the chattering of system is studied in comparison with other standard SMC methods. The simulation results and the THD of the current input of the control system from the other standard SMC methods are greater than the results from the proposed SMC method as shown in Table 2. The decreasing harmonic illustrates the effectiveness of the ERRL technique in chattering reduction.

Table 2 Simulation results of the obtained current THD for the ERRL method and other standard SMC methods

Control	Current THD/%
Constant rate RL	19.62
Constant plus proportional rate RL	18.73
Power rate RL	16.82
ERRL	15.46

All algorithms, including the control law, PLL, and SVPWM, are implemented using the STM32F4-Discovery board. The sampling period is set at 100 ms and the switching frequency is 10 kHz. Although this microcontroller supports floating-point calculation, the mathematical manipulation is done using the fixed-point operation to speed up the computation time. The exponential function in the proposed RL is calculated by using a look-up table to minimize the computational delay. In this experiment, the proposed RL parameters, namely k_d and k_q are evaluated from (42) by substituting σ and μ given at 0.7 and 0.8, respectively. For performance comparison, the experiment is also performed on the conventional SMC using the constant rate RL (5) with the same value of K. The converter starts with the U_{dc} reference at 300 V and the load resistance of 300 Ω connected. After reaching

the steady-state, then the load resistance is changed to 150 Ω by connecting another resistor in parallel with the existing load; in other words, the load decreases from 300 Ω to 150 Ω. The experimental results as shown in Fig. 14 and Fig. 15 indicate the waveforms of the DC output voltage and line current with load at 300 Ω and 150 Ω, respectively. At the load 300 Ω, the DC voltage can be controlled under the conditions as shown in Fig. 14 while Fig. 15 shows the reduction of the DC voltage during the changed load from 300 Ω to 150 Ω as the results of the steady-state error.

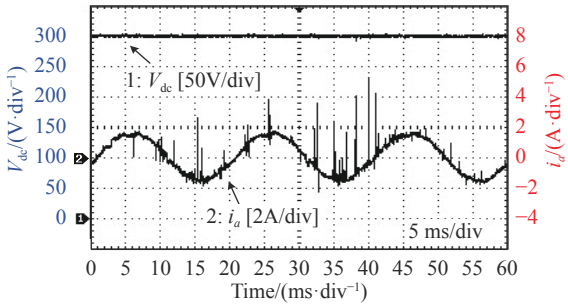

Fig. 14 Steady-state results of the voltage and current: DC output voltage and line current with load at 300 Ω

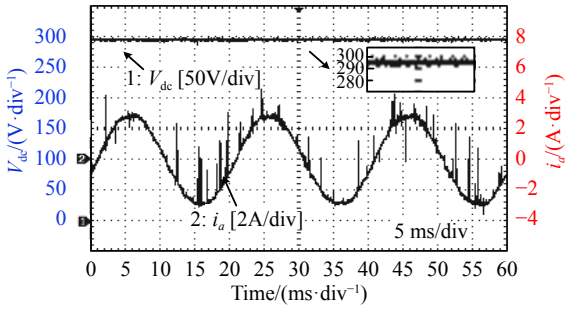

Fig. 15 Steady-state results of the voltage and current: DC output voltage and line current with load at 150 Ω

Fig. 16 (a) and Fig. 16 (b) present the transient response state of the DC voltage and current in the phase A while the load changes from 300 Ω to 150 Ω and from 150 Ω to 300 Ω, respectively. In the period to reach the steady-state, the current changes very fast in response to the changed load increased from 150 Ω to 300 Ω, whereas the DC voltage can be controlled under the specified control conditions as shown in Fig. 16 (a) and Fig. 16 (b), respectively.

Fig. 17 shows that the proposed SMC method achieves near-unity power factor as a result of the in-phase of the voltage and current waveforms. Fig. 18 indicates that the steady-state errors of the DC output voltage of the converter is eliminated and the DC output voltage trajectory approaches the reference voltage at 300 V as the results with the compensated load current method.

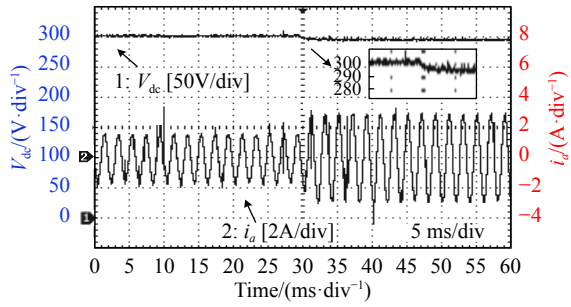

(a) With load from 300 Ω to 150 Ω

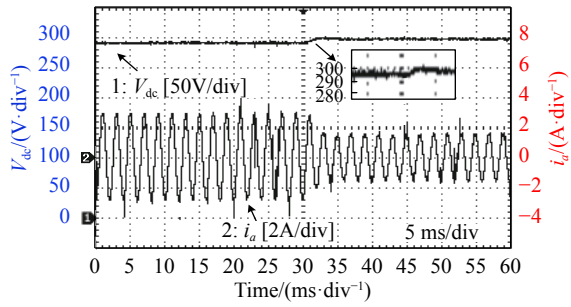

(b) With load from 150 Ω to 300 Ω

Fig. 16 Waveforms of DC output voltage and line current

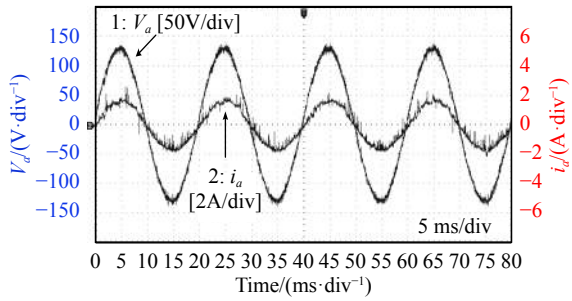

Fig. 17 Waveforms of phase voltage and phase current input with load at 300 Ω

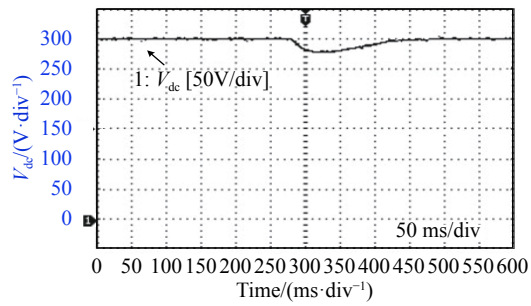

Fig. 18 Test results of the DC output voltage at changed load from 300 Ω to 150 Ω with compensated load current method

The chattering effect occurring in the sliding mode with the controlled three-phase converter via the conventional method and the ERRL method is compared in terms of THD of the current waveforms as presented in Fig. 19 and Fig. 20. Fig. 19 shows that the harmonic level in term of THD of the current waveforms with a conven-

tional method is 22.57 %, while the THD of the current waveforms with the proposed method is 17.13% as shown in Fig. 20. It can be clearly seen that the THD of the proposed SMC is less than those for the conventional SMC, illustrating the effectiveness of the ERRL technique in chattering reduction.

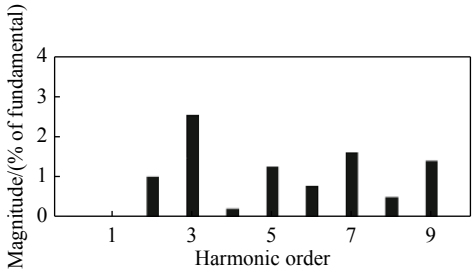

Fig. 19 THD results of the current input: conventional method (Fundamental (50 Hz)=0.4056, THD=22.57%)

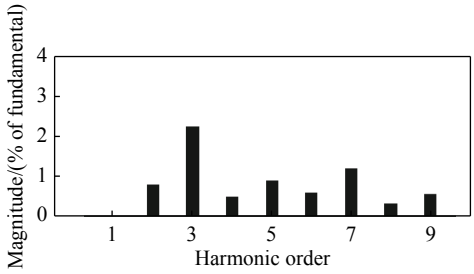

Fig. 20 THD results of the current input: proposed method (Fundamental (50 Hz)=0.41, THD=17.13%)

9. Conclusions

This paper proposes a new technique to control a three-phase AC/DC converter by considering both the control method via SMC and the multi-input control structure. The SMC technique with the ERRL has been discussed. The ERRL structure provides a mechanism for automatically adjusting the effective gain, which is impossible to adjust with the conventional SMC approach. The effective gain increases when the system state is far away from the sliding surface, resulting in fast reaching time. The gain decreases when the system trajectory is in the vicinity of the sliding surface, giving rise to chattering reduction. Each of the ERRL parameters, namely K, σ, and μ, has its own purpose. The parameter μ is for adjusting the chattering level, whereas σ is for specifying the reaching time. The choice of K can be made to maintain the robustness of the system in the face of system uncertainties. The proposed RL is not too complicated in comparison with other RLs, which makes implementation an easy task. The ERRL technique is applied to control the three-phase AC/DC converter with the multi-input control structure. The multi-input control structure reduces the undersigned effect of the time constant and the complexity of the relationship of parameters in each loop that occurs in the cascaded control structure. The experimental results are compared with the results from the conventional SMC under the same experimental conditions. The effect of chattering can be seen from the ripples of the voltage and current waveforms. The comparison shows that the THD of the proposed SMC is less than those for the conventional SMC, illustrating the effectiveness of the ERRL technique in chattering reduction.

References

[1] HEMDANI A, DAGBAGI M, NAOUAR W M, et al. Indirect sliding mode power control for three phase grid connected power converter. IET Power Electronics, 2015, 8(6): 977–985.

[2] HOOSHMAND R A, ATAEI M, REZAEI M H. Improving the dynamic performance of distribution electronic power transformers using sliding mode control. Journal of Power Electronics, 2012, 12(1): 145–156.

[3] LIU J, VAZQUEZ S, WU L, et al. Extended state observer-based sliding-mode control for three-phase power converters. IEEE Trans. on Power Electronics, 2017, 64(1): 22–31.

[4] SHTESSEL Y, BAEV S, BIGLARI H. Unity power factor control in three-phase AC/DC boost converter using sliding modes. IEEE Trans. on Industrial Electronics, 2008, 55(11): 3874–3882.

[5] HE T, LU D D, LI L, et al. Model-predictive sliding-mode control for three-phase AC/DC converters. IEEE Trans. on Power Electronics, 2018, 33(10): 8982–8993.

[6] SLOTINE J J, LI W. Applied nonlinear control. New Jersey: Prentice-Hall, 1991.

[7] UTKIN V I, SHI G J. Sliding mode control in elec-tromechanical systems. London: Taylor and Francis, 2009.

[8] ITKIS U. Control system of variable structure. New York: Wiley, 1976.

[9] SHYU K K, LAI C K. Incremental motion control of synchronous reluctance motor via multisegment sliding mode control method. IEEE Trans. on Control Systems Technology, 2002, 10(2): 169–176.

[10] SIVERT A, FAQIR A, NAHIDMOBARAKEH B, et al. Moving switching surfaces for high precision position control of electrical drives. Proc. of the IEEE International Conference on Industrial Technology, 2004: 175−180.

[11] CHO D, KATO Y, SPILMAN D. Sliding mode and classical controllers in magnetic levitation systems. IEEE Control Systems Magazine, 1993, 13(1): 42–48.

[12] EDWARDS C, SPURGEON K S. Sliding mode control: theory and applications. London: Taylor and Francis, 1998.

[13] UTKIN V I. Variable structure systems with sliding modes. IEEE Trans. on Automatic Control, 1977, 22(2): 212–222.

[14] HUNG J Y, GAO W, HUNG J C. Variable structure control: a survey. IEEE Trans. on Industrial Electronics, 1993, 40(1): 2–22.

[15] CAMACHO O, ROJAS R, GARCIA W. Variable structure control applied to a chemical processes with inverse response. ISA Transactions, 1999, 38(1): 55–72.

[16] QIAO Z W, SHI T N, WANG Y D, et al. New sliding-mode observer for position sensorless control of permanent-magnet synchronouse motor. IEEE Trans. on Industrial Electro-

nics, 2013, 60(2): 710–719.
[17] CHIU J Y C, LEUNG K K S, CHUNG H S H. High-order switching surface in boundary control of inverters. IEEE Trans. on Power Electronics, 2007, 22(5): 1753–1765.
[18] LIN F J, HWANG J C, CHOU P H, et al. FPGA-based intelligent-complementary sliding-mode control for PMLSM servo-drive system. IEEE Trans. on Power Electronics, 2010, 25(10): 2573–2587.
[19] ZHANG X G, ZHAO K, LI S. A PMSM sliding mode control system based on a novel reaching law. Proc. of the International Conference on Electrical Machines and Systems, 2011: 1−5.
[20] ZHAO K, ZHANG X G, LI S, et al. Sliding mode control of high-speed PMSM based on precision linearization control. Proc. of the International Conference on Electrical Machines and Systems, 2011: 1–4.
[21] GAO W, HUNG J C. Variable structure control of nonlinear systems: a new approach. IEEE Trans. on Industrial Electronics, 1993, 40(1): 45–55.
[22] ZHANG X N, VILATHGAMUVA D M, FOO G, et al. Cascaded sliding mode control for global stability of three phase AC/DC PWM rectifier with rapidly varying power electronic loads. Proc. of the 39th Annual Conference of the IEEE Industrial Electronics Society, 2013: 4580−4587.
[23] SI G, ZHAO W, JIA L, et al. Robust sliding mode control of three-phase voltage source PWM rectifier with uncertainties and disturbance. Proc. of the Chinese Control and Decision Conference, 2014: 542−546.
[24] FALLAHA C J, SAAD M, KANAAN H Y, et al. Sliding-mode robot control with exponential reaching law. IEEE Trans. on Industrial Electronics, 2011, 58(2): 600–610.
[25] ASAD M, BHATTI A I, IQBAL S. A novel reaching law for smooth sliding mode control using inverse hyperbolic function. Proc. of the International Conference on Emerging Technologies, 2012: 1−6.
[26] WANG Y Q, FENG Y T, ZHANG X G, et al. A new reaching law for antidisturbance sliding-mode control of PMSM speed regulation system. IEEE Trans. on Power Electronics, 2020, 35(4): 4117–4126.
[27] MOZAYAN S M, SAAD M, VAHEDI H, et al. Sliding mode control of PMSG wind turbine based on enhanced exponential reaching law. IEEE Trans. on Industrial Electronics, 2016, 63(10): 6148–6159.
[28] JEERANANTASIS N, NUNGAM S. New sliding mode control of a three-phase AC/DC converter with exponential rate reaching law. Proc. of the International Electrical Engineering Congress, 2018: 719−722.
[29] KOMURCUGIL H, KUKRER O. Lyapunov-based control for three-phase PWM AC/DC voltage-source converters. IEEE Trans. on Power Electronics, 1998, 13(5): 801−813.

Biographies

JEERANANTASIN Narin was born in 1983. He has received his B.S. and M.S. degrees in electrical engineering from King Mongkut's University of Technology Thonburi, Bangkok, Thailand, in 2004 and 2007, respectively. He is currently pursuing his Ph.D. degree in electrical engineering at King Mongkut's University of North Bangkok. His research interests include nonlinear control and power converters.
E-mail: inc.techcom@gmail.com

NUNGAM Suksun was born in 1960. He received his Ph.D. degree in electrical engineering from National University of Singapore, in 1993. His research interests include nonlinear control and power converters.
E-mail: suksunnungam1@gmail.com